RotateCT: Knowledge Graph Embedding by Rotation and Coordinate Transformation in Complex Space

Yao Dong[1,2], **Lei Wang**[1*], **Ji Xiang**[1], **Xiaobo Guo**[1], **Yuqiang Xie**[1,2]
[1]Institute of Information Engineering, Chinese Academy of Sciences, Beijing, China
[2]School of Cyber Security, University of Chinese Academy of Sciences, Beijing, China
{dongyao,wanglei,xiangji,guoxiaobo,xieyuqiang}@iie.ac.cn

Abstract

Knowledge graph embedding, which aims to learn representations of entities and relations in knowledge graphs, finds applications in various downstream tasks. The key to success of knowledge graph embedding models are the ability to model relation patterns including symmetry/antisymmetry, inversion, commutative composition and non-commutative composition. Although existing methods fail in modeling the non-commutative composition patterns, several approaches support this pattern by modeling beyond Euclidean space and complex space. Nevertheless, expanding to complicated spaces such as quaternion can easily lead to a substantial increase in the amount of parameters, which greatly reduces the computational efficiency. In this paper, we propose a new knowledge graph embedding method called RotateCT, which first transforms the coordinates of each entity, and then represents each relation as a rotation from head entity to tail entity in complex space. By design , RotateCT can infer the non-commutative composition patterns and improve the computational efficiency. Experiments on multiple datasets empirically show that RotateCT outperforms most state-of-the-art methods on link prediction and path query answering.

1 Introduction

Knowledge graphs (KGs) contain structured facts of the real world. Real-world large-scale KGs such as WordNet (Miller, 1995), YAGO (Suchanek et al., 2007), Freebase (Bollacker et al., 2008) and Nell (Mitchell et al., 2018) have been applied to strengthen the performance of several downstream tasks including recommender systems (Zhang et al., 2016), question answering (Hao et al., 2017), conversation generation (Zhou et al., 2018), relation extraction (Vashishth et al., 2018) and machine translation (Zhao et al., 2020). Generally, KGs have the following features: large-scale and incomplete. Therefore, to exploit the semantic information in KGs, predicting missing links based on the existing facts has gained growing interest in recent years. This task can be divided into two categories according to the length of the path: link prediction and path query answering. Link prediction focuses on single-hop reasoning (e.g., answering the path $s \to r \to ?$, where r is a relation), while path query answering (PQA) focuses on multi-hop reasoning (e.g., answering the path query $s \to path \to ?$, where $path$ contains multiple relations).

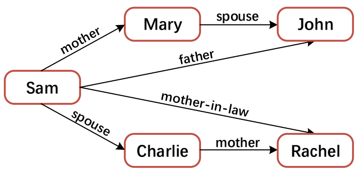

Figure 1: An example in real world. Sam's mother's spouse is John, i.e., Sam's father; Sam's spouse's mother is Rachel, i.e., Sam's mother-in-law. "mother" and "spouse" form a non-commutative composition pattern.

A popular approach for link prediction and PQA is knowledge graph embedding (KGE), which encodes each element in KG into a continuous low-dimensional vector space. The performance of KGE methods greatly relys on the ability of modeling and inferring relation patterns including symmetry/antisymmetry, inversion and composition. In particular, the composition patterns can be further divided into the **commutative composition patterns** and **non-commutative composition patterns**. For example, "spouse" is a symmetric relation and "mother" is an antisymmetric relation. Relations such as "has_part" and "part_of" forms an inversion pattern. The meaning of the composition of "mother" and "spouse" depends on the relative order. By contrast, the composition of "mother" and "mother" has a definite meaning, i.e., "grandmother" (Fig. 1 provides an ex-

*Corresponding author.

ample of the non-commutative composition patterns in real world). Existing methods can capture one or more relation patterns. TransE (Bordes et al., 2013) models antisymmetry, inversion and commutative composition patterns by translating relations from head entities to tail entities. RotatE (Sun et al., 2019), which regards relations as rotations from head entities to tail entities in complex space, can model the symmetry/antisymmetry, inversion and commutative composition patterns. However, most approaches fail to model the non-commutative composition patterns, which is essential for learning more meaningful embeddings. Therefore, quaternion-valued methods such as QuatE (Zhang et al., 2019), Rotate3D (Gao et al., 2020) and DualE (Cao et al., 2021) emerge in sight. By the non-commutativity of quaternion, these methods successfully model the non-commutative composition patterns. Nevertheless, a **quaternion** has two more dimensions than a complex number, which **increases the space cost**. Seeking out a balanced solution that can model the non-commutative composition patterns and maintain a relatively low space cost is pressing.

To address this challenge, we revisit complex space and notice an interesting case: the combination of rotation and coordinate transformation in complex plane is non-commutative, which can empower a KGE method the ability of modeling the non-commutative composition patterns. In addition, the **complex number** is two dimensions less than the quaternion, which **reduces the space cost**.

In this paper, we propose a novel method called **RotateCT** for knowledge graph embedding. Our method first translates the origin of complex plane by a relation-specific displacement. Further, each relation is regarded as a rotation about the new origin of complex plane from head entity to tail entity. By combining rotation and coordinate transformation, RotateCT obtains non-commutativity, which enables RotateCT to effectively model the non-commutative composition patterns.

In summary, our contributions are listed as follows: (1) RotateCT provides an elegant way to model the non-commutative composition patterns and improve the parameter efficiency. To the best of our knowledge, this paper is the first to introduce coordinate transformation into the complex plane for modeling non-commutative composition patterns. (2) We provide comprehensive theoretical analyses on the non-commutative property of combining rotation and coordinate transformation, and discuss the inference patterns, parameter efficiency of RotateCT. (3) Experimental results demonstrate that RotateCT outperforms most baseline approaches on link prediction and path query answering.

2 Related Work

In this section, unlike most papers, we roughly divide the existing KGE methods into three categories according to the non-commutativity and discuss their connections to our approach.

2.1 Models without Non-commutativity

TransE (Bordes et al., 2013) is the most representative KGE model, which embeds both entities and relations as vectors in the same embedding space based on the principle $\mathrm{h} + \mathrm{r} \approx \mathrm{t}$, where $\mathrm{h}, \mathrm{r}, \mathrm{t}$ denote head entity, relation and tail entity, respectively. Several variants (Wang et al., 2014; Lin et al., 2015; Ji et al., 2015; Xiao et al., 2016) are proposed to remedy the limitations of TransE when modeling 1-N, N-1 and N-N relations. In addition, TorusE (Ebisu and Ichise, 2018) models triplets on a torus, which is a Non-Euclidean space. Inspired by Euler's identity $e^{i\theta} = cos\theta + isin\theta$, RotatE (Sun et al., 2019) regards translations as rotations from head entities to tail entities in complex space. Moreover, TransC (Lv et al., 2018) and BoxE (Abboud et al., 2020) encode elements by explicitly defining the regions such as hyperspheres or boxes.

RESCAL (Nickel et al., 2011) is the first bilinear model that can perform collective learning via matching the latent semantics between entities and relations. DistMult (Yang et al., 2015) and ComplEx (Trouillon et al., 2016) are proposed to solve the overfitting problem of RESCAL. In addition, HolE (Nickel et al., 2016) absorbs the quintessence from DistMult and ComplEx. Recently, approaches such as SimplE (Kazemi and Poole, 2018) and TuckER (Balazevic et al., 2019b) turn to different forms of decomposition.

Although some of these methods claim to enable the inference of composition patterns, in practice they cannot infer the non-commutative composition patterns, only support the inference of the commutative composition patterns.

2.2 Models with Non-commutativity

Recently, several approaches explore the usage of more sophisticated spaces to obtain the non-commutativity, which is important for multi-hop reasoning. Specifically, Rotate3D (Gao et al., 2020) and QuatE (Zhang et al., 2019) model relations as rotations in quaternion space with different score functions. DualE (Cao et al., 2021) makes the first attempt to combine rotation and translation by expanding the embedding space to dual quaternion space. DihEdral (Xu and Li, 2019) limits relation matrices to be block diagonal and represents each block with an element in a dihedral group.

Although such approaches take into account the non-commutative composition patterns, they are parameter inefficient due to the complicated vector spaces such as quaternion space.

Our method RotateCT models the non-commutative composition patterns in complex space by introducing the coordinate transformation. Compared to the above three sophisticated spaces, modeling in complex space can significantly improve the parameter efficiency.

2.3 Other Models

Recently, a number of approaches focus on utilizing neural networks. However, the neural networks lack interpretability, and it is difficult to give theoretical analyses from the perspective of inference patterns. Generally, such approaches verify the performance by empirical experiments. ConvE (Dettmers et al., 2018), ConvKB (Nguyen et al., 2018) and InteractE (Vashishth et al., 2020) model the interactions between entities and relations by convolutional neural networks. Additionally, R-GCN (Schlichtkrull et al., 2018) and KBGAT (Nathani et al., 2019) redesign a graph convolutional network and a graph attention network, respectively. Several works tried to exploit more global graph structures like multi-hop paths. Path-RNN (Das et al., 2017) and ROP (Yin et al., 2018) employ RNNs to explicitly model paths. CoKE (Wang et al., 2019) uses a stack of Transformer blocks to model paths.

Compared to the other models, RotateCT is more interpretable, since we can provide comprehensive theoretical analyses of it.

3 Methodology

3.1 RotateCT

Formally, let $\mathcal{E}$ denote the set of entities and $\mathcal{R}$ denote the set of relations. Then a knowledge graph $\mathcal{G}$ is a collection of factual triplets $\{(\mathrm{h}, \mathrm{r}, \mathrm{t})\}$, where $\mathrm{h}, \mathrm{t} \in \mathcal{E}$ and $\mathrm{r} \in \mathcal{R}$. Lowercase letters h, r and

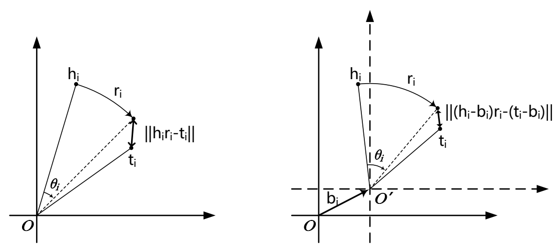

(a) RotatE (b) RotateCT

Figure 2: Illustrations of RotatE and RotateCT in 1 dimension of embeddings. RotatE models r as a rotation. RotateCT models r as a rotation and a displacement, i.e., rotating around the new origin obtained by the displacement.

t denote the head entity, relation and tail entity, respectively; the corresponding boldface letters $\mathbf{h}$, $\mathbf{r}$ and $\mathbf{t}$ denote the embeddings of them. Note that the i-th element of $\mathbf{h}$ is h_i. Let k denote the dimension of entity and relation embeddings.

In this paper, we propose RotateCT to model non-commutative composition patterns in complex space. Inspired by Euler's identity $e^{i\theta} = cos\theta + isin\theta$ and coordinate transformation, our model first projects entities to the complex space, i.e., $\mathbf{h}, \mathbf{t} \in \mathbb{C}^k$. Then we translate the origin of complex planes $\mathbf{O}$ to $\mathbf{O}'$ by a relation-specific displacement $\mathbf{b}$, where $\mathbf{b} \in \mathbb{C}^k$. Further, we define each relation as an element-wise rotation about $\mathbf{O}'$ from head entity $\mathbf{h}$ to tail entity $\mathbf{t}$. In other words, given a golden triplet $(\mathrm{h}, \mathrm{r}, \mathrm{t})$, we expect that:

$$\mathbf{t} - \mathbf{b} = (\mathbf{h} - \mathbf{b}) \circ \mathbf{r}$$

where $\circ$ is the Hadmard (or element-wise) product. Specifically, we have $t_i - b_i = (h_i - b_i)r_i$ for each element of $\mathbf{h}$, $\mathbf{r}$, $\mathbf{t}$ and $\mathbf{b}$. Here, we constrain the modulus of each element of $\mathbf{r} \in \mathbb{C}^k$, i.e., $r_i \in \mathbb{C}$, to be $|r_i| = 1$. Then r_i is of the form $e^{i\theta_i}$, which corresponds a counterclockwise rotation by θ_i radians about the new origin of the complex plane. We define the distance-based score function as follows:

$$d_r(\mathrm{h}, \mathrm{t}) = \sum_{i=1}^{k} \|(h_i - b_i)r_i - (t_i - b_i)\|$$

Optimization. Following Sun et al. (2019), we use a loss function similar to the negative sampling loss (Mikolov et al., 2013) for optimizing:

$$L = -\sum_{i=1}^{m} \frac{1}{m} \log \sigma(d_r(\mathrm{h}'_i, \mathrm{t}'_i) - \gamma) \\ - \log \sigma(\gamma - d_r(\mathrm{h}, \mathrm{t}))$$

where γ is a fixed margin, σ is the sigmoid function, m is the negative sampling size, and $d_r(\mathrm{h}'_i, \mathrm{t}'_i)$ represents the score of i-th negative triplet. We also use the self-adversarial negative sampling (Sun et al., 2019) for drawing negative samples. Specifically, the negative triplets are generated from the following distribution:

$$p(\mathrm{h}'_j, \mathrm{r}, \mathrm{t}'_j | \{(\mathrm{h}_i, \mathrm{r}, \mathrm{t}_i)\}) = \frac{\exp \alpha f_r(\mathrm{h}'_j, \mathrm{t}'_j)}{\sum_i \exp \alpha f_r(\mathrm{h}'_i, \mathrm{t}'_i)}$$

where $f_r(\mathrm{h}'_i, \mathrm{t}'_i) = -d_r(\mathrm{h}'_i, \mathrm{t}'_i)$, α is the temperature of sampling, and $(\mathrm{h}'_i, \mathrm{r}, \mathrm{t}'_i)$ denotes the i-th negative triplet. The modified loss function with self-adversarial negative sampling is as follows:

$$L = -\sum_{i=1}^{m} p(\mathrm{h}'_i, \mathrm{r}, \mathrm{t}'_i) \log \sigma(d_r(\mathrm{h}'_i, \mathrm{t}'_i) - \gamma) \\ - \log \sigma(\gamma - d_r(\mathrm{h}, \mathrm{t}))$$

In addition, we perform regularization on **h** and **t** to avoid overfitting. Therefore, the final loss function takes the following form:

$$L = -\sum_{i=1}^{m} p(\mathrm{h}'_i, \mathrm{r}, \mathrm{t}'_i) \log \sigma(d_r(\mathrm{h}'_i, \mathrm{t}'_i) - \gamma) \\ - \log \sigma(\gamma - d_r(\mathrm{h}, \mathrm{t})) + \lambda(\|\mathbf{h}\|^2 + \|\mathbf{t}\|^2)$$

where λ is the regularization rate. We utilize Adam (Kingma and Ba, 2014) as the optimizer.

3.2 Discussion

In this part, we first introduce the inference patterns and provide some theoretical analyses of RotateCT. Then we discuss the connections between RotateCT and RotatE.

Inference Patterns. Most knowledge graphs mainly consist of three important relation patterns: **symmetry/antisymmetry**, **inversion** and **composition** (commutative composition and non-commutative composition). See formal definitions of inference patterns in Appendix A.

Properties of RotateCT. RotateCT has the non-commutativity and can infer the most common patterns in KG, as stated next.

Theorem 1 *(**Non-commutativity**) The combination of the operations (rotation and coordinate transformation) in RotateCT is non-commutative. (See proof in Appendix B)*

Theorem 2 *(**Inference ability**) RotateCT can infer the **symmetry/antisymmetry**, **inversion** and **composition** patterns. (See proof in Appendix C. We provide illustrations of RocateCT modeling symmetry and non-commutative composition patterns in Appendix D.)*

Connections to RotatE. Combining rotation and coordinate transformation enables RotateCT to model the non-commutative composition patterns, which RotatE cannot. Fig. 2 provides illustrations of RotatE and RotateCT with only 1- dimensional embedding. RotatE can be viewed as a special case of RotateCT. Specifically, RotateCT will degenerate into RotatE when the displacement $\mathbf{b} = \mathbf{0}$.

4 Experiments

We evaluate RotateCT on two common tasks: link prediction (Bordes et al., 2013) and path query answering (Guu et al., 2015). In addition, we give analyses about the computational efficiency between RotatCT and Rotate3D.

4.1 Link Prediction

Link prediction aims to predict the missing h or t for a triplet (h, r, t), i.e., predicting the head query $? \rightarrow r \rightarrow t$ or the tail query $h \rightarrow r \rightarrow ?$. Thus, link prediction is a single-hop reasoning task.

Datasets. We evaluate RotateCT on four well-established benchmarks: WN18 (Bordes et al., 2013), FB15k (Bordes et al., 2013), WN18RR (Dettmers et al., 2018) and FB15k-237 (Toutanova and Chen, 2015). Please refer to Appendix F for the details of the four benchmarks.

Evaluation Protocol. Similar to most previous models, the link prediction performance of RotateCT is reported on three standard evaluation metrics: Mean Rank (MR), Mean Reciprocal Rank (MRR) and Hits@N, where $N = 1, 3, 10$. MR is the average rank of all correct entites. MRR is the mean reciprocal rank of all correct entities. Hits@N represents the proportion of correct entities whose rank is not larger than N. A lower MR,

	WN18					FB15k				
Model	MR	MRR	Hits@1	Hits@3	Hits@10	MR	MRR	Hits@1	Hits@3	Hits@10
Models without non-commutativity										
TransE (2013)	-	0.495	0.113	0.888	0.943	-	0.463	0.297	0.578	0.749
DistMult (2015)	655	0.797	-	-	0.946	42	0.798	-	-	**0.893**
ComplEx (2016)	-	0.941	0.936	0.945	0.947	-	0.692	0.599	0.759	0.840
SimplE (2018)	-	0.942	0.939	0.944	0.947	-	0.727	0.660	0.773	0.838
TorusE (2018)	-	0.947	0.943	0.950	0.954	-	0.733	0.674	0.771	0.832
RotatE (2019)	309	0.949	0.944	0.952	0.959	40	**0.797**	**0.746**	0.830	0.884
Other models										
ConvE (2018)	374	0.943	0.935	0.946	0.956	51	0.657	0.558	0.723	0.831
R-GCN+ (2018)	-	0.819	0.697	0.929	**0.964**	-	0.696	0.601	0.760	0.842
NKGE (2018)	336	0.947	0.942	-	0.957	56	0.730	0.650	0.790	0.871
Models with non-commutativity										
DihEdral (2019)	-	0.946	0.942	0.949	0.954	-	0.733	0.641	0.803	0.877
QuatE (2019)	338	0.949	0.941	0.954	0.960	41	0.770	0.700	0.821	0.878
Rotate3D (2020)	214	**0.951**	**0.945**	0.953	0.961	39	0.789	0.728	0.832	0.887
DualE (2021)	-	**0.951**	**0.945**	**0.956**	0.961	-	0.790	0.734	0.829	0.881
RotateCT (ours)	**201**	**0.951**	0.944	**0.956**	0.963	**34**	0.794	0.737	**0.834**	0.888

Table 1: Link prediction results on WN18 and FB15k.

a higher MRR and a higher Hits@N indicate the better performance. Filtered results are reported to avoid possibly flawed evaluation.

Implementation Details. We use PyTorch to implement our model and test it on a Tesla V100 GPU. Hyperparameters of RotateCT are determined via grid search according to the MRR on the validation set. In general, the embedding dimension k is selected in $\{500, 1000\}$; batch size n is searched in $\{512, 1024\}$; the negative sampling size m is picked from $\{256, 512\}$; the fixed margin γ is tuned among $\{6, 9, 12, 24\}$; self-adversarial temperature α is selected from $\{0.5, 1.0\}$. The regularization rate λ is adjusted in $\{0, 0.1\}$. Entity embeddings are uniformly initialized, and the phases of relation embeddings are uniformly initialized between $-\pi$ and π. Both the real and imaginary parts of each dimension in displacement $\mathbf{b}$ are initialized to zero. The best hyperparameters settings and are provided in the Appendix E.

Main Results. We select competitive baselines from the most recent publications with good results reported. Our baselines are categorized into three groups: models without non-commutativity, models with non-commutativity and other models, which is consistent with the Section 2.

The empirical results on four benchmarks are reported in Table 1 and Table 2. The best results are in bold and second best results are underlined. We can see that RotateCT outperforms all the baselines on WN18 and WN18RR, and achieves extremely competitive performance on FB15k and FB15k-237. On WN18RR and FB15k-237, the main relation patterns are symmetry/antisymmetry and composition, which validates the effectiveness of combining rotation and coordinate transformation for inferring the non-commutative composition patterns. On WN18 and FB15k, the main relation patterns are symmetry/antisymmetry and inversion. Since RotateCT has no obvious superiority over other state-of-the-art baselines in modeling symmetry/antisymmetry and inversion patterns, the performance improvement is not significant on WN18 and FB15k. Although DihEdral, QuatE, Rotate3D and DualE can model the non-commutative composition patterns, the link prediction performance of these models is still inferior to RotateCT, which indicates that parameter efficiency is crucial. Note that RotateCT, as a complex-valued method, outperforms the quaternion-valued method Rotate3D on all datasets across most metrics, which fully demonstrates that the combination of rotation and coordinate transformation can effectively model the non-commutative composition patterns.

4.2 Path Query Answering

This task is to answer path queries on KGs (Guu et al., 2015). Given a path query q consisting of a start entity s and a path p, the answer of q is the entities that can be reached from s via p. A path p is a sequence of relations, i.e., $r_1 \rightarrow \ldots \rightarrow r_j$, where j is the length of p. Link prediction can be viewed as a special case of path query answering when the

	WN18RR					FB15k-237				
Model	MR	MRR	Hits@1	Hits@3	Hits@10	MR	MRR	Hits@1	Hits@3	Hits@10
Models without non-commutativity										
TransE (2013)	3384	0.226	-	-	0.501	357	0.294	-	-	0.465
DistMult (2015)	5100	0.430	0.390	0.440	0.490	254	0.241	0.155	0.263	0.419
ComplEx (2016)	5261	0.440	0.410	0.460	0.510	339	0.247	0.158	0.275	0.428
MuRP (2019a)	-	0.475	0.436	0.487	0.554	-	0.336	0.245	0.370	0.521
RotatE (2019)	3340	0.476	0.428	0.492	0.571	177	0.338	0.241	0.375	0.533
BoxE (2020)	**3207**	0.451	0.400	0.472	0.541	**163**	0.337	0.238	0.374	0.538
Other models										
ConvE (2018)	4187	0.430	0.400	0.440	0.520	244	0.325	0.237	0.356	0.501
R-GCN+ (2018)	-	-	-	-	-	-	0.249	0.151	0.264	0.417
NKGE (2018)	4170	0.450	0.421	0.465	0.526	237	0.330	0.241	0.365	0.510
Models with non-commutativity										
DihEdral (2019)	-	0.486	0.442	0.505	0.557	-	0.320	0.230	0.353	0.502
QuatE (2019)	3472	0.481	0.436	0.500	0.564	176	0.311	0.221	0.342	0.495
Rotate3D (2020)	3328	0.489	0.442	0.505	**0.579**	165	**0.347**	0.250	**0.385**	**0.543**
DualE (2021)	-	0.482	0.440	0.500	0.561	-	0.330	0.237	0.363	0.518
RotateCT (ours)	3285	**0.492**	**0.448**	**0.507**	**0.579**	171	**0.347**	**0.251**	0.382	0.537

Table 2: Link prediction results on WN18RR and FB15k-237.

path length is 1. By contrast, path query answering requires more ability of muti-hop reasoning, in which inferring the composition patterns is crucial.

Datasets. We conduct experiments on two datasets released by Guu et al. (2015), which are extracted from WordNet (Miller, 1995) and Freebase (Bollacker et al., 2008). Both datasets contain triplets and paths. Paths are generated from triplets by random walks. The maximum of path length is 5. Paths used for training are only generated from training triplets, while paths used for test are generated from both training triplets and test triplets. Test paths which appear in training paths are removed. Note that paths of length 1 are not sampled, but created by directly adding triplets. Details of generating paths can be found in (Guu et al., 2015). See details of these two datasets in Appendix G.

Evaluation Protocol. We use the same evaluation protocol as in (Guu et al., 2015). Specifically, for each test path $p_t = s \to r_1 \to ... \to r_j \to o$, the corresponding query q is $s \to r_1 \to ... \to r_j \to ?$. Details of evaluation protocol for PQA can be found in Appendix H. We report the mean quantile (MQ) and Hits@10. MQ is the average quantile of all test paths. Hits@10 is the percentage of target answers whose rank is not larger than 10. An excellent model should achieve a higher MQ and a higher Hits@10.

Implementation Details. We train RotateCT with all paths in the training set, which is denoted as "Comp" in (Guu et al., 2015). Note that triplets

	WordNet		Freebase	
Model	MQ	Hits@10	MQ	Hits@10
Implicitly model paths				
Bilinear$^\sharp$	0.894	0.543	0.835	0.421
DistMult$^\sharp$	0.904	0.311	0.848	0.386
TransE$^\sharp$	0.933	0.435	0.880	0.505
RotatE$^\sharp$	0.947	0.653	0.901	0.601
Rotate3D$^\sharp$	**0.949**	0.671	0.905	0.621
RotateCT$^\sharp$ (ours)	**0.949**	0.673	0.907	0.630
Explicitly model paths				
ROP†	-	-	0.907	0.567
CoKE‡	0.942	**0.674**	**0.948**	**0.764**

Table 3: Path query answering results on WordNet and Freebase. [$\sharp$]: Models do not use extra structures to model paths; [$\dagger$]: Model uses **RNN** to model paths; [$\ddagger$]: Model uses **Transformer** to model paths. Best results are in **bold** and second best results are underlined.

are the paths of length 1. To make the results directly comparable, we follow Gao et al. (2020) to train RotateCT on paths of length 1 to 5 in turn, i.e., we train our model on paths of length i until convergence before training on paths of length $i + 1$. Hyperparameters are determined via grid search according to the MQ on the validation set. In general, the embedding dimension k is selected in {500, 1000}; batch size n is searched in {512, 1024}; the negative sampling size m is picked from {256, 512}; the fixed margin γ is tuned among {6, 9, 12, 24}; self-adversarial temperature α is selected from {1.0, 2.0, 3.0}. The regularization rate λ is adjusted in {0, 0.1}. The initialization methods and experimental environment are the same as in link

Model	Rotate3D	RotateCT
Space	$\mathbb{H}^k$	$\mathbb{C}^k$
Dimension	1000	1000
FB15k	48.89M	33.94M(↓ 30.6%)
FB15k-237	44.33M	29.79M(↓ 32.8%)
WN18	122.89M	81.94M(↓ 33.3%)
WN18RR	122.86M	81.92M(↓ 33.3%)
Freebase	225.17M	150.13M(↓ 33.3%)
WordNet	115.69M	77.14M(↓ 33.3%)

Table 4: Number of free parameters.

	Rotate3D	RotateCT
WN18	158s	65s
WN18RR	159s	65s
FB15k	147s	56s
FB15k-237	153s	53s
WordNet	85s	57s
Freebase	103s	68s

Table 5: Training time per 1000 steps of Rotat3D and RotateCT on all datasets.

prediction. The best hyperparameters settings of RotateCT are provided in the Appendix E.

Main Results. Baselines are divided into two categories according to whether they use extra structures to model paths. The first category including Bilinear (Nickel et al., 2011), DistMult (Yang et al., 2015), TransE (Bordes et al., 2013), RotatE (Sun et al., 2019) and Rotate3D (Gao et al., 2020) has no extra structure to model paths; another category including ROP (Yin et al., 2018) and CoKE (Wang et al., 2019) uses RNN or Transformer to model paths.

Table 3 shows experimental results on the two datasets. Compared with methods that implicitly model paths, RotateCT achieves better performance on both WordNet and Freebase, which demonstrates the ability of RotateCT to model the composition patterns. Overall, RotateCT significantly outperforms Bilinear, DistMult, TransE and RotatE. The reason why RotateCT slightly surpasses Rotate3D is that both RotateCT and Rotate3D have the ability of inferring the non-commutative composition patterns. Compared with methods that explicitly model paths, RotateCT outperforms ROP and still obtains results comparable to CoKE on WordNet. Notably, CoKE uses Transformer as an extra structure to model paths, which is a remarkable architecture for natural language process tasks.

In addition to the overall MQ and Hits@10, we further report the results for different path lengths in Appendix K.

4.3 Analyses

Space Efficiency. To compare the space cost of Rotate3D and RotateCT, we caculate out the number of free parameters over different datasets. Results are shown in Table 4, from which we observe that RotateCT with same dimension reduces up to 30% parameters on all datasets. Intuitively, Rotate3D utilizes quaternions to model relations as rotations in 3D space. However, a quaternion has two more dimensions than a complex number, which sharply increases the space cost of Rotate3D.

Time Efficiency. To further compare the training cost of Rotate3D and RotateCT, we report the training time per 1000 steps on all datasets with embedding dimension $k = 1000$. From Table 5, we can find that RotateCT takes much less training time than Rotate3D on all datasets, which confirms the time efficiency superiority of RotateCT. Experiments of training time are performed on an Intel(R) Xeon(R) Silver 4114 CPU at 2.20GHz and a single NVIDIA Tesla V100 32GB GPU.

5 Case Studies

To verify that RotateCT can effectively model all the three types of relation patterns, we provide case studies via histograms on symmetry/antisymmetry and inversion patterns, and some intuitive examples on composition patterns.

5.1 Symmetry/Antisymmetry

Corollary 1 *Based on Theorem 2, if* r *is a symmetric relation, then* $\theta_i = 0 \vee \pm\pi$*; if* r *is an antisymmetric relation, then* $\theta_i \neq 0, \pm\pi$*. (See proof in Appendix I)*

According to the Corollary 1, the phase of each element in the embeddings of a symmetric relation r should be 0 or $\pm\pi$. Otherwise, the phases should not be 0 and $\pm\pi$. We investigate the phases of elements in relation embeddings from a RotateCT trained on WN18 and a RotateCT trained on FB15k-237 with their best hyperparameters in link prediction. The two models are trained with the setting $k = 1000$. Results are shown in Fig. 3. Specifically, Fig. 3(a)-3(b) give the histograms of the two symmetric relations in WN18: derivationally_related_form and verb_group, in which most phases of the two relations are either

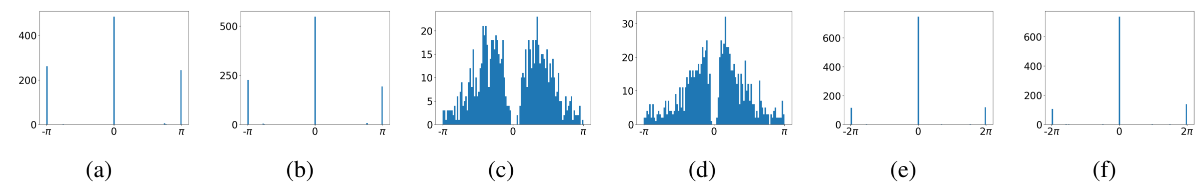

Figure 3: Histograms of relation embeddings phases $\{\theta_{ri}\}(r_i = e^{i\theta_{ri}})$ of two symmetric relations: derivationally_related_form **(a)** and verb_group **(b)**. Histograms of relation embeddings phases $\{\theta_{ri}\}(r_i = e^{i\theta_{ri}})$ of two antisymmetric relations: film/actor/dubbing_performances./film/dubbing_performance/language **(c)** and /people/profession/specialization_of **(d)**. Histograms of the addition of relation embeddings phases $\{\theta_{1i} + \theta_{2i}\}$ of two pairs of inversion relations: has_part ∘ part_of **(e)** and hyponym ∘ hypernym **(f)**, where ∘ is the Hadmard (or element-wise) product.

0 or $\pm\pi$. The above observation confirms that RotateCT can effectively model the symmetry patterns. The histograms of two antisymmetric relations in FB15k-237 are shown in Fig. 3(c)-3(d), from which we can find that the phases of the two antisymmetric relations are scattered. Most phases of the two antisymmetric relations are neither 0 nor $\pm\pi$, which confirms that RotateCT can effectively model the antisymmetry patterns.

5.2 Inversion

Corollary 2 *Based on Theorem 2, if* r_1 *is the inverse of* r_2*, then* $\theta_{1i} + \theta_{2i} = 0 \vee \pm 2\pi$*. (See proof in Appendix J)*

According to the Corollary 2, if r_1 is inverse to r_2, the additive embedding phases, i.e., $\theta_{1i} + \theta_{2i}$, should be 0 or $\pm 2\pi$. Same RotateCT model trained on WN18 in Section 5.1 is used for investigating. Fig. 3(e)-3(f) show the element-wise addition of the embedding phases of two pairs of inverse relations: has_part and part_of, hyponym and hypernym. We can find that most additive embedding phases are either 0 or $\pm 2\pi$, which confirms that RotateCT can effectively model the inversion patterns.

5.3 Composition

To illustrate the superiority of RotateCT in modeling the composition patterns, we use a RotateCT and a RotatE, both trained with their best hyperparameters on the Freebase dataset in path query answering. Fig. 4 shows a subgraph extracted from the Freebase dataset. This subgraph includes two non-commutative composition patterns: "parents' spouse" and "spouse's parents", and one commutative composition pattern: "parents' parents".

Non-commutative Composition. From Fig. 5, we find that RotateCT predicts the query $Maria \rightarrow parents \rightarrow spouse$? and the query $Maria \rightarrow spouse \rightarrow parents$? correctly, which indicates that RotateCT can effectively model the non-commutative composition patterns. However, we observe that RotatE gives unsatisfactory answers in predicting the query $Maria \rightarrow parents \rightarrow$? and the query $Maria \rightarrow spouse \rightarrow parents \rightarrow$?, which verifies that RotatE lacks the ability of inferring the non-commutative composition patterns.

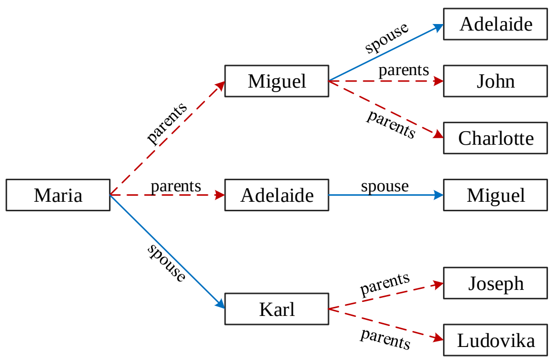

Figure 4: A subgraph about Maria's family. Maria's parents' spouse are Adelaide and Miguel; Maria's spouse's parents are Joseph and Ludovika; Maria's parents's parents are John and Charlotte. Dashed orange arrows represent the parents relation; solid blue arrows represent the spouse relation.

Commutative Composition. We further investigate the ability of inferring the commutative composition patterns of RotateCT and RotatE. As shown in Fig. 5, RotateCT predicts the query $Maria \rightarrow parents \rightarrow parents \rightarrow$? correctly, which confirms that RotateCT can effectively model the commutative composition patterns. By comparision, RotatE fails in predicting the correct answers, i.e., first item in results is not Maria's parents' parents. We argue that this is related to the inability of RotatE to model the non-commutative composition patterns, which has a negative impact

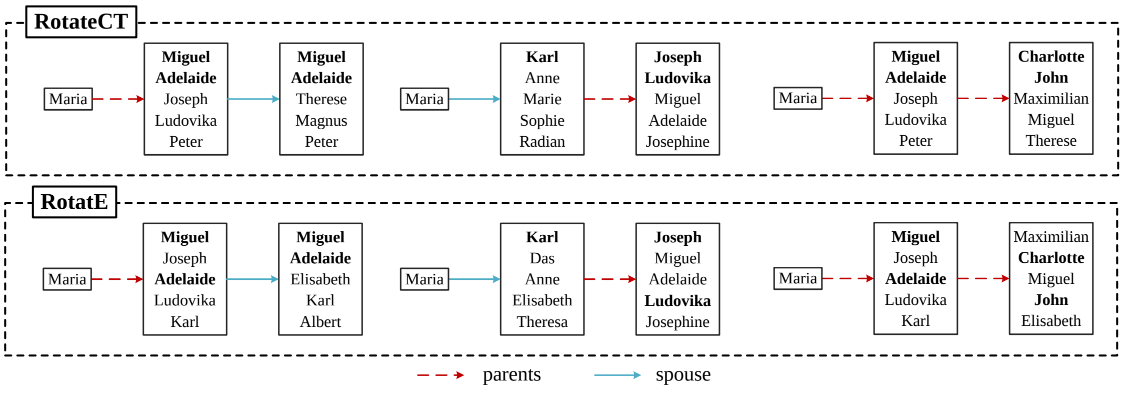
RotateCT
Maria
Miguel Adelaide Joseph Ludovika Peter
Miguel Adelaide Therese Magnus Peter
Maria
Karl Anne Marie Sophie Radian
Joseph Ludovika Miguel Adelaide Josephine
Maria
Miguel Adelaide Joseph Ludovika Peter
Charlotte John Maximilian Miguel Therese
RotatE
Maria
Miguel Joseph Adelaide Ludovika Karl
Miguel Adelaide Elisabeth Karl Albert
Maria
Karl Das Anne Elisabeth Theresa
Joseph Miguel Adelaide Ludovika Josephine
Maria
Miguel Joseph Adelaide Ludovika Karl
Maximilian Charlotte Miguel John Elisabeth
parents
spouse

Figure 5: Top 5 answers of RotateCT and RotatE for three queries: "Who are Maria's parents' spouse?", "Who are Maria's spouse's parents?" and "Who are Maria's parents' parents?". Correct answers are in **bold**.

on embeddings' learning. If RotatE encodes "parents' spouse" and "spouse's parents" in the same way, some semantic information will be lost. This flaw is harmful for RotatE effectively learning the semantics of parents and spouse, which reduces RotatE's performance on modeling the commutative composition pattern "parents' parents".

6 Conclusion

In this paper, we propose a novel knowledge graph embedding method called RotateCT to model the non-commutative composition patterns while improve the parameter efficiency against quaternion-valued methods. RotateCT transforms the coordinates of each entity by translating the origin of coordinates. Further, relations are represented as rotations from head entities to tail entities in complex space. Combining rotation and coordinate transformation empowers RotateCT to model not only commutative composition patterns but also non-commutative composition patterns. As a complex-valued method, the space cost of RotateCT is lower than quaternion-valued methods. Experimental results on link prediction and path query answering show that RotateCT achieves significant performance and demonstrate the superiority of RotateCT for inferring composition patterns. The parameter efficiency analysis proves that RotateCT can reduce the space cost.

In future work, we will explore different ways to model the non-commutative composition patterns and plan to study the combination of quaternion and coordinate transformation.

Acknowledgements

This work was supported by the National Key Research and Development Program of China.

References

Ralph Abboud, Ismail Ceylan, Thomas Lukasiewicz, and Tommaso Salvatori. 2020. BoxE: A box embedding model for knowledge base completion. In *NeurIPS*, volume 33.

Ivana Balazevic, Carl Allen, and Timothy Hospedales. 2019a. Multi-relational poincaré graph embeddings. *NeurIPS*, 32:4463–4473.

Ivana Balazevic, Carl Allen, and Timothy Hospedales. 2019b. TuckER: Tensor factorization for knowledge graph completion. In *EMNLP*, pages 5185–5194.

Kurt Bollacker, Colin Evans, Praveen Paritosh, Tim Sturge, and Jamie Taylor. 2008. Freebase: a collaboratively created graph database for structuring human knowledge. In *SIGMOD*, pages 1247–1250.

Antoine Bordes, Nicolas Usunier, Alberto Garcia-Duran, Jason Weston, and Oksana Yakhnenko. 2013. Translating embeddings for modeling multi-relational data. In *NeurIPS*, volume 26, pages 2787–2795.

Zongsheng Cao, Qianqian Xu, Zhiyong Yang, Xiaochun Cao, and Qingming Huang. 2021. Dual quaternion knowledge graph embeddings. In *AAAI*, volume 35, pages 6894–6902.

Rajarshi Das, Arvind Neelakantan, David Belanger, and Andrew McCallum. 2017. Chains of reasoning over entities, relations, and text using recurrent neural networks. In *EACL*, pages 132–141.

Tim Dettmers, Pasquale Minervini, Pontus Stenetorp, and Sebastian Riedel. 2018. Convolutional 2d knowledge graph embeddings. In *AAAI*, volume 32.

Takuma Ebisu and Ryutaro Ichise. 2018. Toruse: Knowledge graph embedding on a lie group. In *AAAI*, volume 32.

Chang Gao, Chengjie Sun, Lili Shan, Lei Lin, and Mingjiang Wang. 2020. Rotate3d: Representing relations as rotations in three-dimensional space for knowledge graph embedding. In *CIKM*, pages 385–394.

Kelvin Guu, John Miller, and Percy Liang. 2015. Traversing knowledge graphs in vector space. In *EMNLP*, pages 318–327.

Yanchao Hao, Yuanzhe Zhang, Kang Liu, Shizhu He, Zhanyi Liu, Hua Wu, and Jun Zhao. 2017. An end-to-end model for question answering over knowledge base with cross-attention combining global knowledge. In *ACL*, pages 221–231.

Guoliang Ji, Shizhu He, Liheng Xu, Kang Liu, and Jun Zhao. 2015. Knowledge graph embedding via dynamic mapping matrix. In *ACL*, pages 687–696.

Seyed Mehran Kazemi and David Poole. 2018. Simple embedding for link prediction in knowledge graphs. In *NeurIPS*, pages 4284–4295.

Diederik P Kingma and Jimmy Ba. 2014. Adam: A method for stochastic optimization. *arXiv preprint arXiv:1412.6980*.

Yankai Lin, Zhiyuan Liu, Maosong Sun, Yang Liu, and Xuan Zhu. 2015. Learning entity and relation embeddings for knowledge graph completion. In *AAAI*, volume 29.

Xin Lv, Lei Hou, Juanzi Li, and Zhiyuan Liu. 2018. Differentiating concepts and instances for knowledge graph embedding. In *EMNLP*, pages 1971–1979.

Tomas Mikolov, Ilya Sutskever, Kai Chen, Greg S Corrado, and Jeff Dean. 2013. Distributed representations of words and phrases and their compositionality. In *NeurIPS*, pages 3111–3119.

George A Miller. 1995. Wordnet: a lexical database for english. *Communications of the ACM*, 38(11):39–41.

Tom Mitchell, William Cohen, Estevam Hruschka, Partha Talukdar, Bishan Yang, Justin Betteridge, Andrew Carlson, Bhavana Dalvi, Matt Gardner, Bryan Kisiel, et al. 2018. Never-ending learning. *Communications of the ACM*, 61(5):103–115.

Deepak Nathani, Jatin Chauhan, Charu Sharma, and Manohar Kaul. 2019. Learning attention-based embeddings for relation prediction in knowledge graphs. In *ACL*, pages 4710–4723.

Tu Dinh Nguyen, Dat Quoc Nguyen, Dinh Phung, et al. 2018. A novel embedding model for knowledge base completion based on convolutional neural network. In *NAACL*, pages 327–333.

Maximilian Nickel, Lorenzo Rosasco, and Tomaso Poggio. 2016. Holographic embeddings of knowledge graphs. In *AAAI*, volume 30.

Maximilian Nickel, Volker Tresp, and Hans-Peter Kriegel. 2011. A three-way model for collective learning on multi-relational data. In *ICML*, volume 11, pages 809–816.

Michael Schlichtkrull, Thomas N Kipf, Peter Bloem, Rianne Van Den Berg, Ivan Titov, and Max Welling. 2018. Modeling relational data with graph convolutional networks. In *ESWC*, pages 593–607. Springer.

Fabian M Suchanek, Gjergji Kasneci, and Gerhard Weikum. 2007. Yago: a core of semantic knowledge. In *WWW*, pages 697–706.

Zhiqing Sun, Zhi-Hong Deng, Jian-Yun Nie, and Jian Tang. 2019. Rotate: Knowledge graph embedding by relational rotation in complex space. In *ICLR*.

Kristina Toutanova and Danqi Chen. 2015. Observed versus latent features for knowledge base and text inference. In *Proceedings of the 3rd Workshop on Continuous Vector Space Models and their Compositionality*, pages 57–66.

Théo Trouillon, Johannes Welbl, Sebastian Riedel, Éric Gaussier, and Guillaume Bouchard. 2016. Complex embeddings for simple link prediction. In *ICML*.

Shikhar Vashishth, Rishabh Joshi, Sai Suman Prayaga, Chiranjib Bhattacharyya, and Partha Talukdar. 2018. Reside: Improving distantly-supervised neural relation extraction using side information. In *EMNLP*, pages 1257–1266.

Shikhar Vashishth, Soumya Sanyal, Vikram Nitin, Nilesh Agrawal, and Partha P Talukdar. 2020. Interacte: Improving convolution-based knowledge graph embeddings by increasing feature interactions. In *AAAI*, pages 3009–3016.

Kai Wang, Yu Liu, Xiujuan Xu, and Dan Lin. 2018. Knowledge graph embedding with entity neighbors and deep memory network. *arXiv preprint arXiv:1808.03752*.

Quan Wang, Pingping Huang, Haifeng Wang, Songtai Dai, Wenbin Jiang, Jing Liu, Yajuan Lyu, Yong Zhu, and Hua Wu. 2019. Coke: Contextualized knowledge graph embedding. *arXiv preprint arXiv:1911.02168*.

Zhen Wang, Jianwen Zhang, Jianlin Feng, and Zheng Chen. 2014. Knowledge graph embedding by translating on hyperplanes. In *AAAI*, volume 28.

Han Xiao, Minlie Huang, and Xiaoyan Zhu. 2016. From one point to a manifold: knowledge graph embedding for precise link prediction. In *IJCAI*, pages 1315–1321.

Canran Xu and Ruijiang Li. 2019. Relation embedding with dihedral group in knowledge graph. In *ACL*, pages 263–272.

Bishan Yang, Wen tau Yih, Xiaodong He, Jianfeng Gao, and Li Deng. 2015. Embedding entities and relations for learning and inference in knowledge bases.

Wenpeng Yin, Yadollah Yaghoobzadeh, and Hinrich Schütze. 2018. Recurrent one-hop predictions for reasoning over knowledge graphs. In *COLING*, pages 2369–2378.

Fuzheng Zhang, Nicholas Jing Yuan, Defu Lian, Xing Xie, and Wei-Ying Ma. 2016. Collaborative knowledge base embedding for recommender systems. In *SIGKDD*, pages 353–362.

Shuai Zhang, Yi Tay, Lina Yao, and Qi Liu. 2019. Quaternion knowledge graph embeddings. In *NeurIPS*, pages 2735–2745.

Yang Zhao, Jiajun Zhang, Yu Zhou, and Chengqing Zong. 2020. Knowledge graphs enhanced neural machine translation. In *IJCAI*, pages 4039–4045.

Hao Zhou, Tom Young, Minlie Huang, Haizhou Zhao, Jingfang Xu, and Xiaoyan Zhu. 2018. Commonsense knowledge aware conversation generation with graph attention. In *IJCAI*, pages 4623–4629.

A Definitions of Inference Patterns

We give the formal definitions of inference patterns as follows:

Definition 1 *A relation* r *is* ***symmetric (antisymmetric)*** *if*

$$\forall \mathrm{x}, \mathrm{y} \in \mathcal{E}, \mathrm{r}(\mathrm{x}, \mathrm{y}) \Rightarrow \mathrm{r}(\mathrm{y}, \mathrm{x}) \; (\, \mathrm{r}(\mathrm{x}, \mathrm{y}) \Rightarrow \neg \mathrm{r}(\mathrm{y}, \mathrm{x})\,)$$

A relation with such form is a ***symmetry (antisymmetry)*** *pattern.*

Definition 2 *Relation* r_1 *is* ***inverse*** *to* r_2 *if*

$$\forall \mathrm{x}, \mathrm{y} \in \mathcal{E}, \mathrm{r}_2(\mathrm{x}, \mathrm{y}) \Rightarrow \mathrm{r}_1(\mathrm{y}, \mathrm{x})$$

Relations with such form is an ***inversion*** *pattern.*

Definition 3 *Realtion* r_1 *is* ***composed*** *of relation* r_2 *and relation* r_3 *if*

$$\forall \mathrm{x}, \mathrm{y}, \mathrm{z} \in \mathcal{E}, \mathrm{r}_2(\mathrm{x}, \mathrm{y}) \wedge \mathrm{r}_3(\mathrm{y}, \mathrm{z}) \Rightarrow \mathrm{r}_1(\mathrm{x}, \mathrm{z})$$

r_2 *and* r_3 *are commutative if*

$$\forall \mathrm{x}, \mathrm{y} \in \mathcal{E}, \mathrm{r}_2 \odot \mathrm{r}_3(\mathrm{x}, \mathrm{y}) \Rightarrow \mathrm{r}_3 \odot \mathrm{r}_2(\mathrm{x}, \mathrm{y})$$

r_2 *and* r_3 *are non-commutative if*

$$\forall \mathrm{x}, \mathrm{y} \in \mathcal{E}, \mathrm{r}_2 \odot \mathrm{r}_3(\mathrm{x}, \mathrm{y}) \nRightarrow \mathrm{r}_3 \odot \mathrm{r}_2(\mathrm{x}, \mathrm{y})$$

where $\odot$ *is the composition operator.*

Relations with such form is a ***composition*** *pattern.*

B Proof of Theorem 1

Proof 1 *Given* $\mathrm{r}_1, \mathrm{r}_2 \in \mathcal{R}$ *and* $\mathrm{x} \in \mathcal{E}$, *we have*

$$\begin{aligned} r_{1i} \odot r_{2i}(x_i) =& ((x_i - b_{1i})r_{1i} + b_{1i} - b_{2i})r_{2i} \\ =& x_i r_{1i} r_{2i} - b_{1i} r_{1i} r_{2i} + \\ & b_{1i} r_{2i} - b_{2i} r_{2i}, \qquad (1) \\ r_{2i} \odot r_{1i}(x_i) =& ((x_i - b_{2i})r_{2i} + b_{2i} - b_{1i})r_{1i} \\ =& x_i r_{1i} r_{2i} - b_{2i} r_{1i} r_{2i} + \\ & b_{2i} r_{1i} - b_{1i} r_{1i}. \qquad (2) \end{aligned}$$

Apparently, Equation (1) is not equal to (2), which means that the combination of operations in RotateCT is non-commutative. If and only if $b_{1i} = b_{2i}$ *or* $r_{1i}r_{2i} = r_{1i} + r_{2i}$, $r_{1i} \odot r_{2i}(x_i) = r_{2i} \odot r_{1i}(x_i)$.

C Proof of Theorem 2

Proof 2 *For the* ***symmetry/antisymmetry*** *pattern, given* $\mathrm{r} \in \mathcal{R}$ *and* $\mathrm{x}, \mathrm{y} \in \mathcal{E}$, *if* $\mathrm{r}(\mathrm{x}, \mathrm{y})$ *and* $\mathrm{r}(\mathrm{y}, \mathrm{x})$ *hold, we have*

$$\begin{cases} y_i - b_i = (x_i - b_i)r_i \\ x_i - b_i = (y_i - b_i)r_i \end{cases} \Rightarrow \quad r_i = \pm 1$$

Otherwise, if $\mathrm{r}(\mathrm{x}, \mathrm{y})$ *and* $\neg \mathrm{r}(\mathrm{y}, \mathrm{x})$ *hold, we have*

$$\begin{cases} y_i - b_i = (x_i - b_i)r_i \\ x_i - b_i \neq (y_i - b_i)r_i \end{cases} \Rightarrow \quad r_i \neq \pm 1$$

For the ***inversion*** *pattern, given* $\mathrm{r}_1, \mathrm{r}_2 \in \mathcal{R}$ *and* $\mathrm{x}, \mathrm{y} \in \mathcal{E}$, *if* $\mathrm{r}_1(\mathrm{y}, \mathrm{x})$ *and* $\mathrm{r}_2(\mathrm{x}, \mathrm{y})$ *hold, we have*

$$\begin{cases} x_i - b_{1i} = (y_i - b_{1i})r_{1i} \\ y_i - b_{2i} = (x_i - b_{2i})r_{2i} \end{cases}$$

$$\Rightarrow \begin{cases} r_{1i} r_{2i} = 1 \\ b_{1i} = b_{2i} \end{cases} \quad or \quad r_{1i} = r_{2i} = 1$$

For the ***composition*** *pattern, given* $\mathrm{r}_1, \mathrm{r}_2, \mathrm{r}_3 \in \mathcal{R}$ *and* $\mathrm{x}, \mathrm{y}, \mathrm{z} \in \mathcal{E}$, *if* $\mathrm{r}_1(\mathrm{x}, \mathrm{z})$, $\mathrm{r}_2(\mathrm{x}, \mathrm{y})$ *and* $\mathrm{r}_3(\mathrm{y}, \mathrm{z})$ *hold, we have*

$$\begin{cases} z_i - b_{1i} = (x_i - b_{1i})r_{1i} \\ y_i - b_{2i} = (x_i - b_{2i})r_{2i} \\ z_i - b_{3i} = (x_i - b_{3i})r_{3i} \end{cases}$$

$$\Rightarrow \begin{cases} r_{1i} r_{2i} = r_{3i} \\ b_{1i} r_{1i} r_{2i} = b_{1i} r_{2i} - b_{2i} r_{2i} + b_{3i} r_{3i} \end{cases}$$

if r_2 *and* r_3 *are commutative, then*

$$b_{2i} = b_{3i} \quad or \quad r_{2i} r_{3i} = r_{2i} + r_{3i},$$

if r_2 *and* r_3 *are non-commutative, then*

$$\begin{cases} b_{2i} \neq b_{3i} \\ r_{2i} r_{3i} \neq r_{2i} + r_{3i} \end{cases}$$

In conclusion, RotateCT can infer ***symmetry/antisymmetry***, ***inversion*** *and* ***composition*** *patterns.*

D Illustrations of RotateCT

Fig. 6 shows illustrations of RocateCT modeling symmetry and non-commutative composition patterns.

Dataset	embedding dimension	batch size	self-adversarial temperature	margin	negative sample size	distance	regularization/rate	learning rate
WN18	1000	512	0.5	12	256	L1	L1/0.1	1×10^{-4}
WN18RR	1000	1024	1.0	6	512	L1	L1/0.1	5×10^{-5}
FB15k	1000	1024	0.5	24	256	L2	-	2×10^{-4}
FB15k-237	1000	1024	1.0	12	256	L2	-	2×10^{-4}
WordNet	1000	512	1.0	6	256	L2	L2/0.1	5×10^{-5}
Freebase	1000	1024	2.0	12	512	L2	-	2×10^{-5}

Table 6: Hyperparameters setting of RotateCT over different datasets.

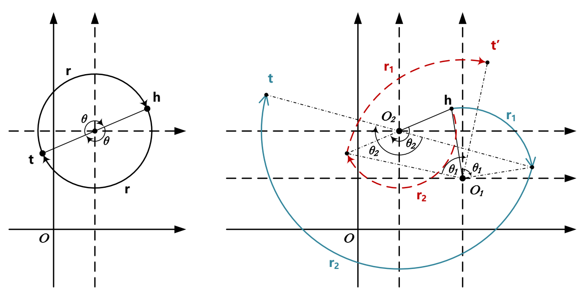

(a) Symmetry (b) Non-commutative composition

Figure 6: Illustrations of RotateCT over two relation patterns. Fig. 6(a) shows how RotateCT models the symmetry pattern, i.e., $r = \pm 1$. In 6(b), blue solid lines represent the path $h \rightarrow r_1 \rightarrow r_2 \rightarrow t$ and red dashed lines represent the path $h \rightarrow r_2 \rightarrow r_1 \rightarrow t'$. r_1 and r_2 form a non-commutative composition pattern. When the relative order of r_1 and r_2 changes, RotateCT can get two different entities: t and t'.

E Hyperparameters Settings

We list the best hyperparameters setting of RotateCT on all datasets in Table 6.

F Details of Link Prediction Datasets

WN18 is a subset of WordNet (Miller, 1995), a database consisting of lexical relations between words. FB15k is extracted from Freebase (Bollacker et al., 2008), a large-scale knowledge graph containing general facts. The main relation patterns in WN18 and FB15k are **symmetry/antisymmetry** and **inversion** (Sun et al., 2019). However, both WN18 and FB15k suffer from test leakage through inverse relations (Toutanova and Chen, 2015). To avoid this problem, WN18RR and FB15k-237 remove the inverse relations in WN18 and FB15k, respectively. Therefore, the main relation patterns in WN18RR and FB15k-237 are **symmetry/antisymmetry** and **composition** (Sun et al., 2019). Notably, semantic information in WN18RR and FB15k-237 is more difficult to capture on account of removing the inverse relations. The statistics of the benchmarks for link prediction are listed in Table 7.

Dataset	#entity	#relation	#training	#validation	#test
FB15k	14,951	1,345	483,142	50,000	59,071
WN18	40,943	18	141,442	5,000	5,000
FB15k-237	14,541	237	272,115	17,535	20,466
WN18RR	40,943	11	86,835	3,034	3,134

Table 7: Number of entities, relations, and triplets in each split for four benchmarks.

G Details of Path Query Answering Datasets

The statistics of path query answering datasets are summarized in Table 8.

	WordNet	**Freebase**
#Entities	38,551	75,043
#Relations	11	13
#Train Triplets	110,361	316,232
#Valid Triplets	2,602	5,908
#Test Triplets	10,462	23,733
#Train Paths	2,129,539	6,266,058
#Valid Paths	11,277	27,163
#Test Paths	46,577	109,577

Table 8: Number of entities, relations, triples and paths in each split of the two datasets.

H Evaluation Protocol of PQA

For each test path $p_t = s \rightarrow r_1 \rightarrow \ldots \rightarrow r_j \rightarrow o$, the corresponding query q is $s \rightarrow r_1 \rightarrow \ldots \rightarrow r_j \rightarrow ?$. For each query q, the candidate answers are entities that "type-match", i.e., all tail entities of the final relation r_j. The correct answers are entities that can be reached from s by traversing the path p; the incorrect answers are obtained by filtering out the correct answers from the candidate answers. The set of candidate answers to a query q denotes as $\mathcal{C}(q)$; the set of correct answers to a query q denotes as $\mathcal{P}(q)$; the set of incorrect answers to a query q denotes as $\mathcal{N}(q)$. We give the formal definition of $\mathcal{C}(q)$, $\mathcal{P}(q)$, and $\mathcal{N}(q)$ as follows:

$$\begin{aligned}
\mathcal{C}(q) &\triangleq \{o|\exists e \text{ s.t. } (e, r_j, o) \in \mathcal{G}\} \\
\mathcal{P}(q) &\triangleq \{o|\exists e_1, ..., e_{j-1} \text{ s.t. } (s, r_1, e_1), \\
&\qquad ..., (e_{j-1}, r_j, o) \in \mathcal{G}\} \\
\mathcal{N}(q) &\triangleq \mathcal{C}(q) \backslash \mathcal{P}(q)
\end{aligned}$$

Here $\mathcal{G}$ includes training triplets and test triplets. For each test path p_t, we replace entity o with entities in $\mathcal{C}(q)$ and compute the score of each candidate answer. Then we rank the scores of candidates along with the score of p_t in descending order and caculate the quantile, which is the proportion of incorrect answers ranked after the target answer o.

Notably, some test paths in both datasets are "type-match trivial", i.e., all type matching candidate answers are correct. Hence, the quantile of these test paths are undefined, and we exclude them from evaluation.

I Proof of Corollary 1

Proof 3 *As shown in Theorem 2, if* r *is a symmetric relation, we have*

$$\begin{aligned}
r_i = \pm 1 &\Rightarrow cos\theta_i + isin\theta_i = \pm 1 \\
&\Rightarrow cos\theta_i = \pm 1 \\
&\Rightarrow \theta_i = 0 \vee \pm\pi
\end{aligned}$$

Otherwise, if r *is an antisymmetric relation, we have*

$$\begin{aligned}
r_i \neq \pm 1 &\Rightarrow cos\theta_i + isin\theta_i \neq \pm 1 \\
&\Rightarrow cos\theta_i \neq \pm 1 \\
&\Rightarrow \theta_i \neq 0, \pm\pi
\end{aligned}$$

J Proof of Corollary 2

Proof 4 *As shown in Theorem 2, if* r_1 *is the inverse of* r_2*, we have*

$$\begin{cases} r_{1i} r_{2i} = 1 \\ b_{1i} = b_{2i} \end{cases} \quad or \quad r_{1i} = r_{2i} = 1$$

In the first case, we have

$$\begin{cases} r_{1i} r_{2i} = 1 \\ b_{1i} = b_{2i} \end{cases}$$

$$\Rightarrow \begin{cases} (cos\theta_{1i} + isin\theta_{1i})(cos\theta_{2i} + isin\theta_{2i}) = 1 \\ b_{1i} = b_{2i} \end{cases}$$

$$\Rightarrow \begin{cases} cos(\theta_{1i} + \theta_{2i}) + isin(\theta_{1i} + \theta_{2i}) = 1 \\ b_{1i} = b_{2i} \end{cases}$$

$$\Rightarrow \begin{cases} \theta_{1i} + \theta_{2i} = 0 \vee \pm 2\pi \\ b_{1i} = b_{2i} \end{cases}$$

In the second case, we have

$$\begin{aligned}
r_{1i} = r_{2i} = 1 &\Rightarrow cos\theta_{1i} + isin\theta_{1i} = \\
&\quad\;\; cos\theta_{2i} + isin\theta_{2i} = 1 \\
&\Rightarrow \theta_{1i} = \theta_{2i} = 0
\end{aligned}$$

Combining the above two cases, we have

$$\theta_{1i} + \theta_{2i} = 0 \vee \pm 2\pi$$

K PQA Results of Different Path Lengths

We further report the path query answering results for different path lengths. As shown in Table 9 and Table 10, RotateCT outperforms RotatE and Rotate3D over most metrics, which verifies the superior capability of RotateCT to deal with the multi-hop reasoning.

	length=1		length=2		length=3		length=4		length=5	
Model	MQ	Hits@10	MQ	Hits@10	MQ	Hits@10	MQ	Hits@10	MQ	Hits@10
RotatE	**0.934**	0.794	0.882	0.403	0.922	0.649	0.858	0.415	0.910	0.652
Rotate3D	0.933	0.796	**0.901**	**0.473**	0.921	0.685	0.854	0.449	0.908	0.654
RotateCT	**0.934**	**0.803**	0.885	0.460	**0.928**	**0.707**	**0.863**	**0.462**	**0.920**	**0.689**

Table 9: Path query answering results of each path length on Freebase. Best results are in **bold**.

	length=1		length=2		length=3		length=4		length=5	
Model	MQ	Hits@10	MQ	Hits@10	MQ	Hits@10	MQ	Hits@10	MQ	Hits@10
RotatE	0.868	0.350	0.970	0.786	0.973	0.778	0.970	0.737	0.967	0.693
Rotate3D	**0.872**	**0.365**	**0.972**	0.797	0.974	0.786	**0.973**	0.750	0.969	0.706
RotateCT	0.865	0.338	**0.972**	**0.807**	**0.975**	**0.796**	**0.973**	**0.763**	**0.971**	**0.731**

Table 10: Path query answering results of each path length on WordNet. Best results are in **bold**.